Search for High Mass Photon Pairs in $p\overline{p} \to \gamma\gamma jj$ Events at $\sqrt{s} = 1.8$ TeV

The DØ Collaboration *
Fermi National Accelerator Laboratory, Batavia, Illinois 60510
(June 18, 1999)

Abstract

A search has been carried out for events in the channel $p\overline{p} \to \gamma\gamma jj$. Such a signature can characterize the production of a non-standard Higgs boson together with a W or Z boson. We refer to this non-standard Higgs, having standard model couplings to vector bosons but no coupling to fermions, as a "bosonic Higgs." With the requirement of two high transverse energy photons and two jets, the diphoton mass ($m_{\gamma\gamma}$) distribution is consistent with expected background. A 90(95)% C.L. upper limit on the cross section as a function of mass is calculated, ranging from 0.60(0.80) pb for $m_{\gamma\gamma} = 65$ GeV/c^2 to 0.26(0.34) pb for $m_{\gamma\gamma} = 150$ GeV/c^2, corresponding to a 95% C.L. lower limit on the mass of a bosonic Higgs of 78.5 GeV/c^2.

*Submitted to the *International Europhysics Conference* on *High Energy Physics*, *EPS-HEP99*, 15 – 21 July, 1999, Tampere, Finland.

The Higgs sector of the standard model is poorly constrained. Several extended Higgs models [1–6] allow a light neutral scalar Higgs with suppressed couplings to fermions. We refer to such a non-standard Higgs, having standard model couplings to vector bosons but zero couplings to fermions, as a "bosonic Higgs." The model of Refs. [1,2] provides a bosonic Higgs without requiring fine tuning and maintains the relation $\rho = M_W^2/M_Z^2 \cos^2\theta_W = 1$, consistent with present experimental limits [7].

The decay channels of a bosonic Higgs differ from those of the standard model Higgs as shown in Fig. 1. Since the fermion decay channels are suppressed, the decay of a bosonic Higgs with mass less than $2M_W$ is not dominated by $H \to b\bar{b}$. At tree level the bosonic Higgs decays only to $WW^{(*)}$ and $ZZ^{(*)}$ vector bosons (where the asterisks denote that one or both of the vector bosons may be off the mass shell). For bosonic Higgs masses less than 90 GeV/c^2, the one-loop W-boson-mediated $H \to \gamma\gamma$ channel becomes dominant.

A bosonic Higgs is most easily detected in the associated production mode, where an off-mass-shell W or Z boson is produced and radiates a Higgs boson [8]. Higgs production through vector boson fusion also contributes to the $\gamma\gamma jj$ final state at the 15% level. The sum of the WH and ZH production cross sections ranges from 1.8 pb for $M_H = 60$ GeV/c^2, to 0.4 pb for $M_H = 100$ GeV/c^2. We expect sensitivity in the $\gamma\gamma jj$ final state up to a mass of $M_H \sim 85$ GeV/c^2 for the decay modes $H \to \gamma\gamma$ and $W/Z \to jj$, at which mass the branching ratio $H \to \gamma\gamma$ remains high and the falling Higgs production cross section of $\sim$ 0.4 pb allows the production of tens of events. This Letter describes the first search for a bosonic Higgs at hadron colliders.

Experiments at the LEP collider have previously set lower mass limits on a bosonic Higgs. A limit of approximately 60 GeV/c^2 was established [8,9] in data taken at the Z^0, a higher 95% C.L. limit set at 76.5 GeV/c^2 in 172 GeV collisions [10] at LEP2, and this limit extended to 90.0 GeV/c^2 in 183 GeV collisions. [11]

Data corresponding to an integrated luminosity of $101.2 \pm 5.5\,\mathrm{pb}^{-1}$, recorded during 1992–96 with the DØ detector [12], are used for this analysis. Photons and jets are identified using the uranium-liquid-argon sampling calorimeter, extending to a pseudorapidity $|\eta| = |-\ln\tan\frac{\theta}{2}| \lesssim 4.5$, where θ is the polar angle. The electromagnetic (EM) energy resolution is $\sigma_E/E = 15\%/\sqrt{E(\mathrm{GeV})} \oplus 0.3\%$, and the jet energy resolution is about $\sigma_E/E = 80\%/\sqrt{E(\mathrm{GeV})}$. The calorimeter is segmented transversely into towers in pseudorapidity and azimuthal angle of size $\Delta\eta \times \Delta\phi = 0.1 \times 0.1$, and further segmented to 0.05×0.05 at the EM shower maximum. Drift chambers in front of the calorimeter are used to distinguish photons from electrons. A three-level triggering system is employed: level 0 uses scintillation counters near the beam pipe at each end of the detector to detect an inelastic interaction; level 1 sums the EM and hadronic energy in calorimeter towers of size $\Delta\eta \times \Delta\phi = 0.2 \times 0.2$; and level 2 is a software trigger which forms clusters of calorimeter cells and applies loose cuts on the shower shape.

Events used in this analysis have at least two photon candidates and at least two jet candidates. Initially, the events are selected using a diphoton trigger that requires two EM showers with a transverse energy (E_T) greater than 12 GeV. The filter is fully efficient when both photons have $E_T > 15$ GeV. The offline event selection criteria are optimized by requiring one photon to have $E_T^\gamma > 30\,\mathrm{GeV}$ and $|\eta^\gamma| < 1.1$ or $1.5 < |\eta^\gamma| < 2.0$, and the other to have $E_T^\gamma > 15\,\mathrm{GeV}$ and $|\eta^\gamma| < 1.1$ or $1.5 < |\eta^\gamma| < 2.25$. Additionally, one hadronic

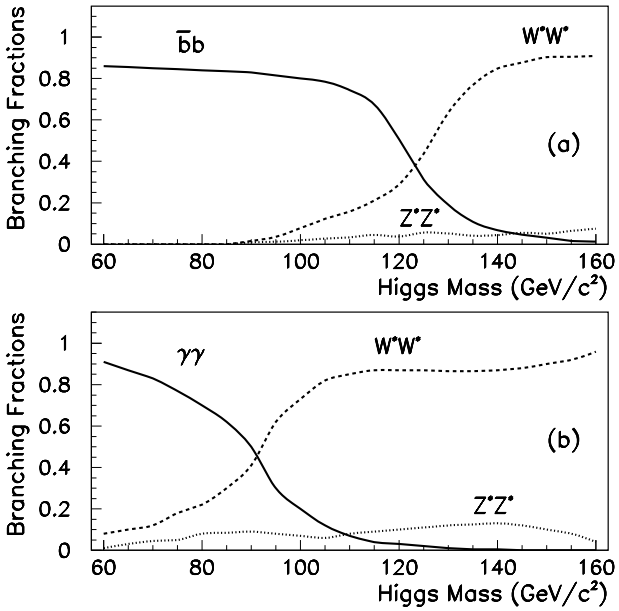

FIG. 1. Decay branching fractions vs. Higgs mass for (a) standard model Higgs, and (b) bosonic Higgs. In (a), the diphoton branching fraction is less than 0.001; $c\bar{c}$ and $\tau^+\tau^-$ Higgs decay channels are not shown. In (b), the Higgs decays to only VV, where V = γ, W, or Z. There is a large enhancement in the diphoton channel for the bosonic Higgs model: the absence of competing decay channels results in a dominant $H \to \gamma\gamma$ below $M_H \approx 90$ GeV/c^2.

jet is required to have $E_T^{\rm jet} > 30\,{\rm GeV}$ and $|\eta^{\rm jet}| < 2.0$, and the other hadronic jet to have $E_T^{\rm jet} > 15\,{\rm GeV}$ and $|\eta^{\rm jet}| < 2.25$. For the two jets to be consistent with the decay of a W or Z boson, the dijet mass is required to be between 40 GeV/c^2 and 150 GeV/c^2. A photon candidate is rejected if there is either a reconstructed track or a significant number of drift chamber hits in a tracking road $\Delta\theta \times \Delta\phi = 0.2 \times 0.2$ between the cluster in the calorimeter and the interaction vertex. A photon candidate is required to have a shower shape consistent with that of a single EM shower, to have more than 96% of its energy in the EM section of the calorimeter, and to be isolated [13]. Isolation requires that the transverse energy in the annular region between $\mathcal{R} \equiv \sqrt{\Delta\eta^2 + \Delta\phi^2} = 0.2$ and $\mathcal{R} = 0.4$ around the cluster be less than 10% of the total cluster transverse energy. In addition, each photon candidate must be separated by $\Delta\mathcal{R}_\gamma > 0.7$ from every jet [14]. Each jet candidate is reconstructed from energy deposited in a $\Delta\mathcal{R} < 0.7$ cone, must have less than 95% of its energy in the EM section of the calorimeter, and must have no more than 40% of its energy in the outermost layer of the hadronic portion of the calorimeter.

These selection criteria yield four events, whose $m_{\gamma\gamma}$ distribution is shown in Fig. 2a. No events are observed with $m_{\gamma\gamma} > 60$ GeV/c^2. The resolution of the detector in $m_{\gamma\gamma}$ is about 2.5 GeV/c^2 for diphoton final states passing these kinematic cuts. The corresponding dijet mass distributions of data and expected background are shown in Fig. 2b.

The dominant background to the $\gamma\gamma jj$ channel is production of QCD multijet events in which two jets are misidentified as photons. During the jet fragmentation process, π^0 and η mesons are produced and decay promptly into multiple photons. If the π^0 or η meson carries a large fraction of the jet energy and has a momentum greater than about 10

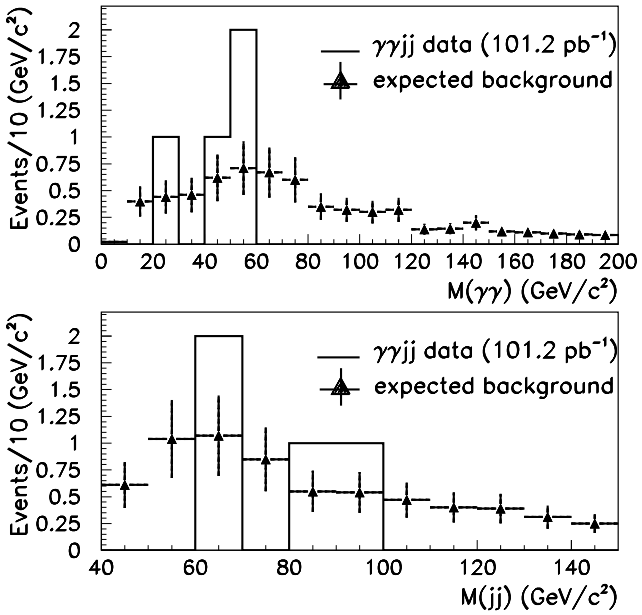

FIG. 2. The data and expected background for (a) the diphoton mass and (b) the dijet mass distributions.

GeV/c the decay photons coalesce to mimic a single isolated photon in the calorimeter. The depth development of multiple photons differs from that of a single photon, and a fit to the longitudinal shower shape for photon candidates yields the probability $P(j \rightarrow \text{“}\gamma\text{”})$ for a jet to mimic an isolated photon candidate, estimated to be $(4.3 \pm 1.0) \times 10^{-4}$, with a weak E_T dependence [14].

Smaller sources of background are from double direct photon production, single direct photon production with one jet fluctuating into a photon candidate, and final states containing electrons in addition to two jets, such as $(W \rightarrow e^{\pm}\nu)\gamma jj$, $(Z \rightarrow e^+e^-)jj$, and $t\bar{t} \rightarrow e^+e^-\nu\nu jj$, where the electrons fail track reconstruction and are misidentified as photons. By rejecting events that have a track or significant number of drift chamber hits inside the tracking road, the expected electron background is reduced to less than 0.01 events, and is not considered further.

The QCD multijet background to $\gamma\gamma jj$ events is estimated from the data. Starting with the same trigger and data set as the signal sample, a background sample is selected by requiring two EM clusters and jets satisfying the same kinematic and fiducial criteria as the signal. Both EM clusters are required to have more than 90% of their energy in the EM section of the calorimeter and to have no reconstructed track associated with the cluster, but at least one of the two EM clusters is required to fail the photon quality criteria (isolation, shower shape, or EM fraction). The resulting sample of 194 events is expected to be dominated by QCD multijet events where two jets fluctuate into highly-electromagnetic clusters. After subtracting the expected direct photon event contribution, the QCD multijet background for $m_{\gamma\gamma}$ >60 GeV/c^2 is estimated by normalizing the cluster-pair mass distribution to the signal sample over the mass range $m_{\gamma\gamma}$ <60 GeV/c^2, where bosonic Higgs have been excluded by earlier searches for $Z \rightarrow Z^*H$ at LEP [9,10].

The direct photon background is calculated using the PYTHIA Monte Carlo [15]. This

background has two sources: single direct photon production where one true photon is produced and one jet is misidentified as a photon, and double direct photon production, where two true photons are produced in addition to two high-E_T jets. The Monte Carlo jet and photon energies are smeared to match the measured detector resolutions. The efficiency for the events to pass the photon quality criteria (isolation, shower shape, EM fraction, and tracking) are calculated from data using our $Z \to e^+e^-$ event sample. The single direct photon events are weighted by the probability P($j \to$ "γ"), since one of the jets must be misidentified as a photon for a background event to be accepted. The direct photon background is normalized to the signal sample using the calculated direct photon cross section. The dominant systematic uncertainty in these sources of background then derives from the observed level of agreement between the theoretical and experimental direct photon cross sections, and is estimated to be 40% for double direct photon production and 20% for single direct photon production [13,16].

Figure 2 shows the total expected background, with estimated uncertainties, in bins of 10 GeV/c^2. The total background of 6.0 ± 1.6 events consists of 4.0 ± 1.5 QCD multijet events and 2.0 ± 0.6 direct photon events. It agrees well with our observed number of four events. We find no evidence for non-standard sources of $\gamma\gamma jj$ events. If we increase the photon pseudorapidity coverage to $|\eta^\gamma| < 2.5$, and reduce the leading jet and photon transverse energy requirements to 15 GeV, the same background estimation technique predicts 38 ± 10 events while 39 events are observed. The $m_{\gamma\gamma}$ and m_{jj} distributions of this larger sample are also described well by the estimated background.

Seven samples of bosonic Higgs events, each containing 5000 simulated events, are generated using PYTHIA for the processes $p\bar{p} \to WH$ and $p\bar{p} \to ZH$, with the decays $H \to \gamma\gamma$ and $W/Z \to qq'$, for Higgs masses of 60, 70, 80, 90, 100, 110, and 150 GeV/c^2. These events are processed through the detector simulation and event reconstruction software. The Higgs selection criteria are applied and the signal acceptance and efficiency calculated; their product ranges from 0.06 to 0.10 for Higgs masses of 60 to 150 GeV/c^2. The systematic uncertainty in the acceptance for the Higgs signal is based on the level of agreement between the Monte Carlo and data-based estimates of the photon and jet selection efficiencies. The systematic error includes the uncertainties in the efficiencies for the photon trigger and selection (2%), requirement on photon track rejection (13%), hadronic energy scale (5-11%), EM energy scale ($\simeq$1%), and jet reconstruction ($\simeq$1%). The statistical uncertainty on the Monte Carlo Higgs samples is about 3%. The systematic and statistical uncertainties, and the integrated luminosity uncertainty of 5.3%, are added in quadrature and yield 15%.

The 90% and 95% confidence level (C.L.) limits on the cross section as a function of $m_{\gamma\gamma}$ are shown in Fig. 3 and are calculated using a Bayesian approach [7], incorporating the uncertainties associated with the efficiency, acceptance, luminosity, and the expected background as a function of $m_{\gamma\gamma}$ and m_{jj}. Correlations between errors are negligible and not included. A general 95% C.L. upper limit on the cross section is calculated from the exclusion contour in Fig. 3, and ranges from 0.80 pb for $m_{\gamma\gamma} = 65$ GeV/c^2 to 0.34 pb for $m_{\gamma\gamma} = 150$ GeV/c^2. The corresponding 90% C.L. is noted in the figure. The full bosonic Higgs cross section is also plotted in the Fig. 3, and includes both the associated production and vector boson fusion production processes, calculated using PYTHIA with a QCD correction factor [8] of 1.25. This factor agrees with the ratio between our measured cross section for W boson production [17] and the calculated cross section, 1.23 ± 0.08. We

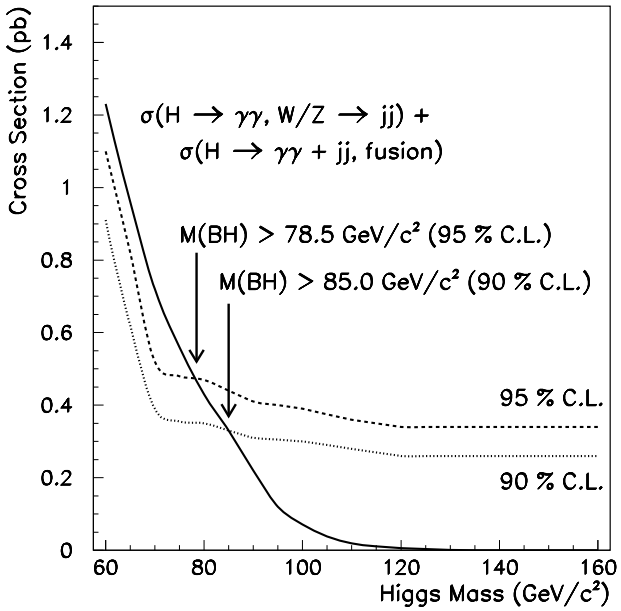

FIG. 3. The solid curve represents the bosonic Higgs 95% C.L. exclusion contour, the dashed curve represents the 90% C.L. exclusion contour, and the dot-dash curve represents the bosonic Higgs cross section with $H \to \gamma\gamma$ and $W/Z \to jj$ branching fractions taken into account.

set lower limits on the bosonic Higgs mass of 85.0 GeV/c^2 at the 90% C.L. and 78.5 GeV/c^2 at the 95% C.L.

In summary, we performed the first search for a bosonic Higgs at hadron colliders, in the channel $p\bar{p} \to \gamma\gamma jj$. Four candidates pass the selection requirements, with an expected background of 6.0 ± 2.1 events. No candidate events are seen with a diphoton mass greater than 60 GeV/c^2. A 95% C.L. bosonic Higgs lower mass limit of 78.5 GeV/c^2 is set, assuming standard model couplings between the Higgs and the vector bosons. The 95% C.L. upper limits on the bosonic Higgs production cross section range from 0.80 pb for $m_{\gamma\gamma} = 65$ GeV/c^2 to 0.34 pb for $m_{\gamma\gamma} = 150$ GeV/c^2.

We thank the Fermilab and collaborating institution staffs for contributions to this work and acknowledge support from the Department of Energy and National Science Foundation (USA), Commissariat à L'Energie Atomique (France), Ministry for Science and Technology and Ministry for Atomic Energy (Russia), CAPES and CNPq (Brazil), Departments of Atomic Energy and Science and Education (India), Colciencias (Colombia), CONACyT (Mexico), Ministry of Education and KOSEF (Korea), and CONICET and UBACyT (Argentina).

REFERENCES

[1] A.G. Akeroyd, Phys. Lett. B **368**, 89 (1996).
[2] A.G. Akeroyd, Phys. Lett. B **353**, 519 (1995).
[3] H.E. Haber, G.L. Kane and T. Sterling, Nucl. Phys. **B161**, 493 (1979).
[4] H. Pois, T. Weiler and T.C. Yuan, Phys. Rev. D **47**, 3886 (1993).
[5] P. Bamert and Z. Kunszt, Phys. Lett. B **306**, 335 (1993).
[6] H. Georgi and M. Machacek, Nucl. Phys. **B262**, 463 (1985); M. Chanowitz and M. Golden, Phys. Lett. **165B**, 105 (1985).
[7] R.M. Barnett *et al.*, Phys. Rev. D **54**, 1 (1996).
[8] A. Stange, W. Marciano and S. Willenbrock, Phys. Rev. D **49**, 1354 (1994).
[9] L3 Collaboration, M. Acciarri *et al.*, Phys. Lett. B **388**, 409 (1996).
[10] OPAL Collaboration, K. Ackerstaff, *et al.*, Eur. Phys. J. **C1** (1998) 31.
[11] OPAL Collaboration, K. Ackerstaff, *et al.*, Phys. Lett. B **437**, 218 (1998).
[12] DØ Collaboration, S. Abachi *et al.*, Nucl. Instrum. Methods Phys. Res. A **338** (1994) 185.
[13] DØ Collaboration, S. Abachi *et al.*, Phys. Rev. Lett. **78**, 2070 (1997).
[14] Bryan A. Lauer, Ph.D. thesis, Iowa State University, Ames, IA (1997), available at `http://www-d0.fnal.gov/results/publications_talks/thesis/lauer/thesis.ps` (unpublished).
[15] T. Sjostrand and M. Bengtsson, Comput. Phys. Commun. **43**, 367 (1987). Version 5.7 was used in this analysis.
[16] W. Chen, Ph.D. Thesis, State University of New York, Stony Brook, NY (1997), available at `http://www-d0. fnal.gov/results/publications_talks/thesis/chen/ - chen.html` (unpublished).
[17] DØ Collaboration, S. Abachi *et al.*, Phys. Rev. Lett. **75**, 1456 (1995).